

Aeroelastic Design of a 25 MW Downwind Rotor for High Efficiency and Low Weight

Michael Jeong¹ and Eric Loth²

University of Virginia, Charlottesville, VA, 22903, USA

Chao (Chris) Qin³

Washington State University, Vancouver, WA, 98686, USA

Michael Selig⁴

University of Illinois Urbana-Champaign, Urbana, IL, 61801, USA

Nick Johnson⁵

Sandia National Laboratories, Albuquerque, NM, 87123, USA

The advantages of continuously increasing wind turbine scales necessitate aeroelastic rotor design strategies to maximize performance. In this study, three downwind 25 MW rotors were designed with an aim of high power production with low rotor weight. To achieve this objective, the swept area was maximized by adjusting pre-cone and shaft tilt angles such that the aeroelastic orientation of an upward pointing blade was nearly vertical near rated conditions. The power coefficient was maximized by using an inverse rotor design tool in which axial induction factor and lift coefficient distributions were prescribed. To determine lift coefficient distributions, a design space was created based on a combination of maximum lift and maximum lift/drag conditions. For the flatback airfoils, empirical correlations were used to adjust for drag and maximum lift coefficient. Once the design space was created, three lift coefficient distributions were chosen which results in three rotors of small, medium, and large chords. The resulting rotors were simulated for performance and optimized for minimum mass using OpenFAST. The results indicated that the medium chord provided the best performance, producing the highest power coefficient and the lowest rotor mass. This approach can be used for other extreme-scale (upwind and downwind) turbines.

I. Nomenclature

| | | |
|------------|---|-----------------------------------|
| c | = | Chord |
| C | = | Coefficient |
| L/D | = | Lift-to-drag ratio |
| N_{crit} | = | Critical number from e^n theory |
| r | = | Local blade radius |
| R | = | Blade radius (root to tip) |
| t | = | Thickness |
| y | = | Deflection |
| Ψ | = | Azimuthal angle |

Subscripts

| | | |
|-----|---|------------|
| d | = | Drag value |
|-----|---|------------|

¹ Graduate Research Assistant (Ph.D. Candidate), Department of Mechanical and Aerospace Engineering, mwj2pf@virginia.edu.

² Professor, Department of Mechanical and Aerospace Engineering, loth@virginia.edu, Fellow, AIAA.

³ Assistant Professor, School of Engineering and Computer Science, chris.qin@wsu.edu, Member AIAA.

⁴ Professor, Department of Aerospace Engineering, m-selig@illinois.edu, Associate Fellow, AIAA.

⁵ Wind Technology and Design Manager, Wind Energy Design and Experimentation Department, najohns@sandia.gov.

- l = Lift value
- max = Maximum value
- P = Power value
- TE = Trailing edge value
- tip = Blade tip value
- 0 = Zero angle of attack value

II. Introduction

The escalating global demand for energy has led to the fast growth of renewable energy, which offers a cleaner and environmentally-friendly source of energy that can help mitigate growing environmental challenges. Wind energy is expected to become one of the leading renewable energy sources and efforts to grow the wind energy sector are focusing more on offshore opportunities. In 2021, the Biden Administration announce a 30 GW target for offshore wind in the Unites States [1]. Offshore wind presents an opportunity for more energy production due to more abundant wind resources. Extreme-scale wind turbines can better capture energy from offshore wind than smaller wind turbines due to its increased swept area [2],[3]. In addition to increases in turbine scale, downwind rotors can be more advantageous than conventional upwind rotors by allowing for more flexible and thus lighter blades as there is less potential for tower strike [4]. However, extreme-scale turbines still pose unprecedented structural challenges to limit the blade loads and deflections that occur from longer blades, higher offshore wind speeds, and higher levels of turbulence. Using conventional rotor design methods may result in suboptimal heavy blades that add costs. To that end, robust design methods for extreme-scale turbines are necessary.

In the past, wind turbine blades were often designed using a direct design approach where a blade geometry is first generated before being analyzed for aerodynamic performance and then adjusted in an iterative sequence until the blade geometry that produces the desired performance emerges. This method is more computationally expensive and less efficient than the inverse design approach that is more often used today. In an inverse design approach, desired aerodynamic parameters are first specified, such as C_l distribution or axial induction factor, and used to then iteratively determine a blade geometry that achieves the specified parameters. This removes the need to analyze a blade geometry between each iteration and is well suited to design rotor around peak power production. The inverse design method has been used to design research and commercial turbines and was the method used in this study. Particularly, the inverse design tool PROPID has been used previously for extreme-scale turbine design [5]-[7]. The PROPID tool incorporates a multipoint inverse method and blade-element momentum theory to inversely design blades based on user specified performance characteristics including peak power, axial induction factor, and C_l distribution. It has been used in previous designs of a 13.2 MW and 25 MW rotor [8],[9].

Airfoil selection is an important aspect of wind turbine blade design to maximize power production. The airfoils used to design the blades in this study were the F1 family of airfoils developed by [9] and are shown below in Table 1. Near the blade root, flatback airfoils are used for increased structural support and increased $C_{l,max}$ that they can provide [10]. In designing blades, computational tools like XFOIL are often used to predict airfoil characteristics needed as inputs in an inverse design process. However, numerically obtained two-dimensional airfoil characteristics, such as those obtained from XFOIL or computational fluid dynamics have been shown to mispredict airfoil characteristics of flatback airfoils [11]-[15]. If such airfoil characteristics are used in blade design, the resulting rotors may underperform in real operation. Thus, to consider the limited accuracy of these tools, adjustments should be made at the appropriate Reynolds numbers to ensure that realistic flatback airfoil lift and drag coefficients are used in blade design.

Once an aerodynamic design of a blade is completed, higher fidelity simulations can be used to predict the dynamics of the rotor and give insight into blade loads and deflections that can inform rotor geometry design decisions like pre-cone and shaft tilt angles. Tools like the OpenFAST wind turbine simulation framework exist to perform such simulations [16]. OpenFAST simulations were performed by [8] following their PROPID design phase to observe predicted aeroelastic deflections. Structural design and optimization are also necessary after blades are aerodynamically designed to minimize mass and cost. Along with developing OpenFAST, the National Renewable Energy Laboratory (NREL) has developed the Wind-Plant Integrated System Design & Engineering Model (WISDEM) framework that can quickly optimize the structural design of a blade based on steady state models [17]. The OpenFAST and WISDEM tools are both used in this study following the PROPID design phase.

This paper presents the design of a 25 MW downwind offshore rotor. The focus of the design was on maximizing power production which was achieved using three design stages to maximize swept area by optimizing pre-cone and

shaft tilt angles, and to maximize C_p by optimizing blade chord and twist. In designing blade chord and twist with PROPID, C_l distributions had to be prescribed for which a C_l design space was created to inform these decisions. OpenFAST simulations were run to compare aerodynamic performance of the three rotor designs. WISDEM structural optimization was also performed to compare blade mass. This paper will first cover the PROPID design process, including the development of the C_l design space and novel empirical correlations. Next, OpenFAST simulations will be discussed, followed the WISDEM optimization.






III. Design Methodology

A. Design Parameters

In the first part of the design process, the main design parameters (rotor size, design tip speed ratio, axial induction factor, airfoils) were based on the 25 MW V2e rotor described by [18]. An axial induction factor of 1/3 along the blade span was chosen to maximize aerodynamic performance. As offshore turbine continues to increase in size, higher tip-speed limits may be more appropriate and have already been considered in other extreme-scale turbine designs [18],[19]. Thus, the optimal tip-speed ratio of 9.25 was determined using an aggressive tip-speed limit of 120 m/s. Blade length and hub radius were based on the V2e turbine size. Pre-cone and shaft tilt angles were calculated with a focus on maximizing swept area with rigid blades. In the case of an upward-pointing blade ($\Psi = 0^\circ$), the swept area maximizing configuration is setting the blade vertically. For the downward-pointing blade ($\Psi = 180^\circ$), there are tip deflection limits set by the International Electrotechnical Commission (IEC) 61400-1 standards specifying the minimum distance a blade tip needs to be away from the tower at all times [20]. Considering this limit and the tower designed in [18], the downward-pointing blade could be positioned at 12° away from vertical. Pre-cone and shaft tilt angles were then calculated to achieve this configuration.

The airfoils used in these designs were the F1 family of airfoils ranging from 18%–48% thickness and are shown in Table 1 [9]. XFOIL was used to obtain two-dimensional lift and drag coefficients of the F1 airfoils before then being processed through the AirfoilPrep preprocessor for applied three-dimensional rotational corrections. These XFOIL results assumed free transition with $N_{crit} = 9$. However, because XFOIL has been shown to underpredict C_d and overpredict $C_{l,max}$ for flatback airfoils [9],[13], experimental wind tunnel data for flatback airfoils at Reynolds numbers between 0.76×10^6 to 4×10^6 was collected and then used to empirically adjust the XFOIL data for the F1 airfoils [21]-[26].

Table 1 Thicknesses, zero angle of attack lift coefficient, and normalized span location of F1 airfoils

| Airfoil | t_{max}/c | t_{TE}/c | t_{TE}/t_{max} | C_{l0} | r/R | Airfoil Profile |
|--------------|-------------|------------|------------------|----------|------|---------------------------------------------------------------------------------------|
| F1-4846-1226 | 48.46% | 12.26% | 0.253 | 0.997 | 0.25 |  |
| F1-3856-0738 | 38.56% | 7.38% | 0.191 | 0.781 | 0.35 |  |
| F1-2655-0262 | 26.55% | 2.62% | 0.099 | 0.673 | 0.55 |  |
| F1-2040-0087 | 20.4% | 0.87% | 0.044 | 0.640 | 0.75 |  |
| F1-1822-0041 | 18.22% | 0.41% | 0.023 | 0.605 | 0.95 |  |

From the experimental data, two correlations were found to estimate C_d and $C_{l,max}$. Assuming that C_d is approximately constant before stall for flatback airfoils, C_d was found to correlate with the ratio of the trailing edge thickness to the maximum airfoil thickness. As thinner trailing edge airfoils don't show as significant underprediction

of C_l in XFOIL, this correlation was only used to estimate C_d before stall of airfoils with $t_{TE}/t_{max} > 0.11$. $C_{l,max}$ was found to correlate with C_l at zero angle of attack, representing the effects of airfoil camber. Again, this correlation was only used to adjust the $C_{l,max}$ of thicker flatback airfoils with $t_{max}/c > 26.55\%$ for which XFOIL has been shown to overpredict. These correlations were linearly proportional to the ratio of trailing edge thickness to the maximum thickness, and used for the C_l distributions described in following section.

B. Lift Coefficient Design Space and Distributions

Lift coefficient distribution was one of the inputs used to determine blade chord and twist with the PROPID inverse design tool. To determine a realistic range of C_l values to prescribe C_l distributions from, a design space was created. The upper limit of this design space was based on the $C_{l,max}$ values of the F1 airfoils from XFOIL along the blade span. The lower limit was based on the C_l values at the $(L/D)_{max}$ from XFOIL as well. As shown in Fig. 1a, within the inboard 50% of the blade, high values of $C_{l,max}$ and low values of C_l at $(L/D)_{max}$ are observed due to the limited accuracy of XFOIL for the thicker flatback F1 airfoils. Applying the adjustments described above, more reasonable values of $C_{l,max}$ and increased values of C_l at $(L/D)_{max}$ are observed.

From the adjusted $C_{l,max}$ and $(L/D)_{max}$ curves shown in Fig. 1b, two more adjustments were included to provide a realistic range of C_l values to be used for prescribing C_l distributions. The $C_{l,max}$ curve was uniformly decreased by 0.2 along the entire blade span to consider deviations in angle of attack due to turbulence. The $(L/D)_{max}$ curve was lowered by a factor of 0.6 such that the resulting design space would encompass the adjusted $(L/D)_{max}$ curve since the $(L/D)_{max}$ curve would theoretically be the C_l distribution that would provide the maximum aerodynamic performance. Thus, a reasonable bracket for C_l distributions was created. This design space is shown in green in Fig. 1b.

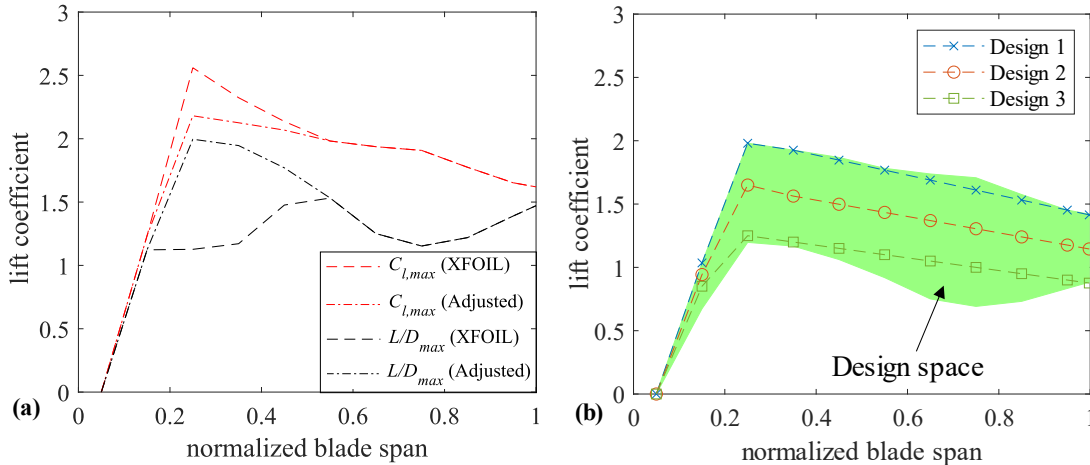


Fig. 1. a) XFOIL maximum lift coefficient and lift-to-drag ratio curves of F1 airfoils for clean conditions b) Lift coefficient distributions of Designs 1–3 within the final design space.

Using this design space, three C_l distributions were determined for each of the three rotor designs, labeled Design 1, Design 2, and Design 3. Each C_l distribution was placed in a different part of the design space, directly leading to differences in blade chord and twist. All three C_l distributions linearly decrease from $r/R = 0.25$ –1. Once the three C_l distributions were determined, PROPID was used to design three rotors, each with a different C_l distribution, which could then be simulated for performance and structural design presented in the following section.

IV. Results and Discussion

A. PROPID Results

The resulting three blade geometries are shown in Fig. 2. All three designs successfully converged the axial induction factor of $1/3$ along the blade span. Each design had a different chord distribution which is inversely related to their respective C_l distributions as expected. Twist distributions shown in Fig. 2b are all similar to each other with greater positive twist angle meaning the blade is twisted to feather. The largest differences in twist occur near the blade

tip with Design 1 showing an increase in twist beyond $r/R = 0.75$ while Designs 2 and 3 continue to decrease in this region. This is the result of maintaining the prescribed C_l distributions in the PROPID tool but was deemed acceptable as the trends in twist at the blade tip appear in order from Design 1 to Design 3 and since the C_l distribution of Design 1 was already at the upper limit of the design space. The maximum C_p estimates from PROPID indicate that Design 2 performed the best with a $C_{p,max}$ of 0.511. However, to further compare Designs 1–3, subsequent OpenFAST simulations and WISDEM structural optimization was completed.

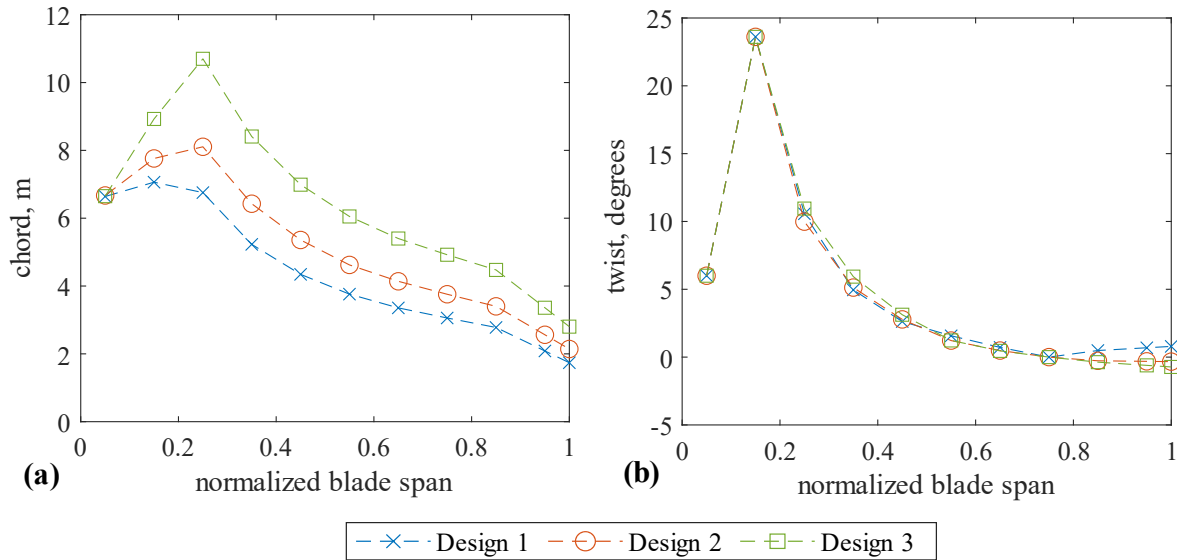


Fig. 2. PROPID results for Designs 1–3 along nondimensional blade span: (a) chord (b) twist.

B. OpenFAST Simulations

OpenFAST simulations were performed using steady Region 2 wind speeds without shear. Since no controller was used, rotor speeds were held constant at each wind speed such that the design tip-speed ratio of 9.25 was maintained. Aerodyn14 module within OpenFAST used for calculating aerodynamic loads based on blade-element momentum theory. Structural properties for the V2e rotor from [18] were used. Both rigid and flexible blade simulations were considered. However, in maintaining the goal of maximizing swept area, the rotor geometry was adjusted for the flexible blade simulations as show in Fig. 3.

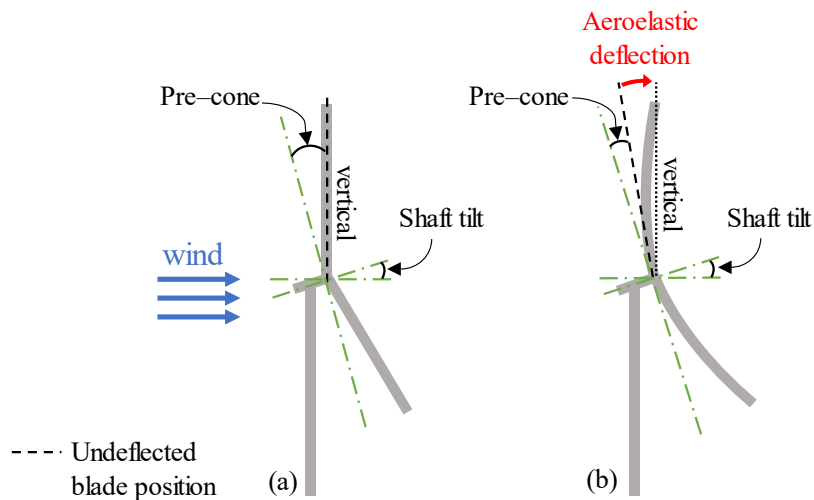


Fig. 3. Pre-cone angle + shaft tilt configurations for OpenFAST simulations: (a) rigid blade case (b) flexible blade case.

Since average blade deflections will bend the blades downwind away from vertical if the rigid configuration is used (shown in Fig. 3a), pre-cone and shaft tilt angles were adjusted such that the undeflected blade position of the blade at $\Psi = 0^\circ$ points slightly upwind. Doing so allows the blade to be positioned nearly vertically when it deflects downwind. This adjustment was based on predictions of blade tip deflections at a steady 8 m/s wind speed under the assumption that the turbine will be operating at a high Region 2 wind speed for the majority of the time. The blade at $\Psi = 180^\circ$ was held at the same location to ensure tip deflection limits are not violated. The resulting pre-cone and shaft tilt angles were 3.6° and 8.4° respectively.

The OpenFAST simulation results predicted Design 2 to generate the most aerodynamic power across the simulated wind speeds while having moderate levels of thrust. On average, Design 2 outperformed Design 1 and Design 3 in terms of power by 0.2%–0.7%. Design 1 showed the highest rated thrust of the three designs at 4.26 MN. These results are consistent with the PROPID results that indicated Design 2 had the highest performance. Introducing blade flexibility with the adjusted pre-cone and shaft tilt angles predicted losses in power and thrust. Design 2 showed losses in aerodynamic power between 1.4%–4.7% and thrust between 0.4% –1.4% across the simulated wind speeds.

C. WISDEM Optimization

The final method of comparing Designs 1–3 was a WISDEM optimization. WISDEM was used to optimize for minimum rotor mass. This optimization was performed after the OpenFAST simulations, meaning the structural properties used for OpenFAST are different than those generated by WISDEM here. Higher fidelity structural designs like the V2e design used in OpenFAST were not possible to complete for Designs 1–3 given time and resource constraints, but the WISDEM results still can provide useful conclusions of the effects of varying blade geometries on rotor mass. Both strain and deflections were constrained in the WISDEM optimization, with spar cap thickness, leading edge thickness, and trailing edge thickness as design variables.

Table 2 WISDEM Blade Mass Optimization Results

| Design | AEP (GWh/yr) | m_{blade} (kg) | y_{tip} (m) |
|--------|--------------|---------------------|---------------|
| 1 | 135.2 | 1.598×10^5 | 41.74 |
| 2 | 135.8 | 1.450×10^5 | 41.63 |
| 3 | 135.5 | 1.532×10^5 | 41.75 |

The WISDEM results shown in Table 2 indicated Design 2 to have the highest annual energy production (AEP) and lowest blade mass, consistent with the PROPID and OpenFAST predictions. The higher $C_{P,max}$ predicted by PROPID likely is the reason for the highest AEP seen from WISDEM. The moderate chord likely limited blade mass and thus costs to a moderate degree. The combination of these two factors is likely the reason Design 2 consistently outperformed Designs 1 and 3. Thus, the design of the 25 MW downwind offshore rotor was completed with Design 2 being recommended for further studies including but not limited to structural analyses and controls design.

VI. Conclusion

The advantages of increased offshore wind turbine scales necessitate the development of robust design strategies that consider the challenges associated with increase blade lengths and masses. In this study, three 25 MW rotors were designed using the PROPID inverse design tool and then compared using OpenFAST simulations and WISDEM optimization to identify the best performing design. A power maximizing approach was used which required the design of rotor geometry to maximize swept area and carefully prescribed C_l distributions to maximize aerodynamic performance. In prescribing C_l distributions, a C_l design space was created that employed novel empirical correlations to adjust inaccurate two-dimensional flatback airfoil characteristics generated using XFOIL. Each rotor design had a different C_l distribution that was located within the developed C_l design space. High-fidelity OpenFAST simulations were run at steady state wind speeds to compare aerodynamic performance of Designs 1–3. Aeroelastic effects were considered. WISDEM structural optimization provided a method to compare rotor mass. The three design stages indicated that Design 2 is the preferred rotor due to: highest $C_{P,max}$ (PROPID), highest power production (OpenFAST),

and lowest blade mass and cost (WISDEM). Although rotor design was completed, this study represents just the first step in designing extreme-scale offshore wind turbines. Further design and analyses are recommended for more detailed structural design and controller design. Further OpenFAST simulations are also recommended following a control system design to verify the performance of these rotors under more realistic or extreme wind conditions. Future studies may also be conducted to better understand the effects of pre-cone and shaft tilt angles on power generation.

Acknowledgments

We would like to acknowledge GE Research and Advanced Research Projects Agency-Energy (ARPA-E), U.S. Department of Energy, for support and input throughout the course of this project as well as ARPA-E for the funding in part under Award Number DE-AR0000667. This work was authored in part by the National Renewable Energy Laboratory, operated by Alliance for Sustainable Energy, LLC, for the U.S. Department of Energy (DOE) under Contract No. DE-AC36-08GO28308. Funding provided by U.S. Department of Energy Advanced Research Projects Agency-Energy. The views expressed in the article do not necessarily represent the views of the DOE or the U.S. Government. The U.S. Government retains a nonexclusive, paid-up, irrevocable, worldwide license to publish or reproduce the published form of this work. M.J. would also like to acknowledge support from the National Science Foundation Research Traineeship (NRT) program under Grant No. 1829004.

References

- [1] The White House, “Biden Administration Jumpstarts Offshore Wind Energy Projects to Create Jobs,” <https://www.whitehouse.gov/briefing-room/statements-releases/2021/03/29/fact-sheet-biden-administration-jumpstarts-offshore-wind-energy-projects-to-create-jobs/>, 2021.
- [2] U.S. Department of Energy (DOE), “Wind Vision: A New Era for Wind Power in the United States,” 2015.
- [3] Shields, M., Beiter, P., Nunemaker, J., Cooperman, A., Duffy, P., “Impacts of turbine and plant upsizing on the levelized cost of energy for offshore wind,” *Applied Energy*, Vol. 298, September 2021, 117189.
- [4] Loth, E., Steele, A., Qin, C., Ichter, B., Selig, M. S., Moriarty, P., “Downwind pre-aligned rotors for extreme-scale wind turbines,” *Wind Energy*, Vol. 20, July 2017, pp. 1129-1311.
- [5] Selig, M. S., Tangler, J. L., “Development and Application of a Multipoint Inverse Design Method for Horizontal Axis Wind Turbines,” *Wind Engineering*, Vol. 19, No. 5, 1995, pp. 91–105.
- [6] Selig, M. S., “PROPID for Horizontal Axis Wind Turbine Design,” <https://m-selig.ae.illinois.edu/propid.html>, 1995-.
- [7] Selig, M. S., “PROPID User Manual Version 5.3.1,” UIUC Applied Aerodynamics Group, 2012.
- [8] Qin, C., Loth, E., Zalkind, D., Pao, L., Yao, S., Griffith, T., Selig, M., Damiani, R., “Downwind Coning Concept Rotor for a 25 MW Offshore Wind Turbine,” *Renewable Energy*, Vol. 156, August 2020, pp. 314-327.
- [9] Ananda, G. K., Bansal S., Selig, M. S., “Aerodynamic Design of the 13.2 MW SUMR-13i Wind Turbine Rotor,” *AIAA Paper 2018-0994*, January 2018. <https://doi.org/10.2514/6.2018-0994>.
- [10] TPI Composites, Inc., “Innovative Design Approaches for Large Wind Turbine Blades,” *Technical Report SAND2004-0074*, Sandia National Laboratories, 2004.
- [11] Drela, M., “XFOIL: An Analysis and Design System for Low Reynolds Number Airfoils,” *Low Reynolds Number Aerodynamics. Lecture Notes in Engineering*, Vol. 54, 1988, pp. 1-12.
- [12] Drela, M., “XFOIL Subsonic Airfoil Development System,” <http://web.mit.edu/drela/Public/web/xfoil/>, 2000- .
- [13] Coder, J. G., Maughmer, M. D., “Comparisons of Theoretical Methods for Predicting Airfoil Aerodynamic Characteristics,” *Journal of Aircraft*, Vol. 51, No. 1, February 2014, pp. 183-191.

- [14] Stone, C., Barone, M., “A Computational Study of the Aerodynamics and Aeroacoustics of a Flatback Airfoil Using Hybrid RANS-LES,” *AIAA Paper 2009-273*, 47th AIAA Aerospace Sciences Meeting, June 2009. <https://doi.org/10.2514/6.2009-273>
- [15] Metzinger, C. N, Chow, R., Baker, J. P., Cooperman, A. M., van Dam, C. P., “Experimental and Computational Investigation of Blunt Trailing-Edge Airfoils with Splitter Plates,” *AIAA Journal*, Vol. 56, No. 8, June 2018. pp. 3229-3239.
- [16] NREL: OpenFAST, v2.5.0, GitHub [code], available at: <https://github.com/OpenFAST/openfast>.
- [17] NREL: WISDEM, v3.2.0, GitHub [code], available at: <https://github.com/WISDEM/WISDEM>.
- [18] Escalera Mendoza, A. S., Griffith, D. T., Qin, C., Loth, E., Johnson, N., “Rapid approach for structural design of the tower and monopile for a series of 25 MW offshore turbines,” *The Science of Making Torque from Wind (TORQUE 2022)*, 2022. <https://doi.org/10.1088/1742-6596/2265/3/032030>
- [19] Yao, S., Cheta, M., Griffith, T. D., Escalera Mendoza, A. S., Selig, M. S., Martin, D., Kianbakht, S., Johnson, K., Loth, E., “Aero-structural design and optimization of 50 MW wind turbine with over 250-m blades,” *Wind Engineering*, Vol 46, July 2021, pp. 273-295.
- [20] International Electrotechnical Commission, “IEC 64100-1, Third Ed. 2005-2008, Wind Turbines – Part I: Design Requirements,” IEC, 2005.
- [21] Berg, D., Barone, M. F., “Aerodynamic and Acoustic Properties of a Flatback Airfoil (Will it Rumble or Whisper),” *Technical Report SAND2008-4306P*, Sandia National Laboratories, 2008.
- [22] Barone, M. F., Berg, D., “Aerodynamic and Aeroacoustic Properties of a Flatback Airfoil: An Update,” *Technical Report SAND2008-8243C*, Sandia National Laboratories, 2008. <https://doi.org/10.2514/6.2009-271>.
- [23] Manolesos, M., Voutsinas, S. G., “Experimental Study of Drag-Reduction Devices on a Flatback Airfoil,” *AIAA Journal*, Vol. 54, No. 11, November 2016, pp. 3382-3396.
- [24] Baker, J. P., van Dam, C. P., Mayda, E. A., “Experimental and Computational Analysis of Thick Flatback Wind Turbine Airfoils,” *AIAA Paper 2006-193*, AIAA Aerospace Sciences Meeting and Exhibit, 2006. <https://doi.org/10.2172/961975>.
- [25] Yilmaz, O., Timmer, W. A., “Experimental Evaluation of a Non-Conventional Flat Back Thick Airfoil Concept for Large Offshore Wind Turbines,” *AIAA Paper 2018-3827*, AIAA Applied Aerodynamic Conference, June 2018. <https://doi.org/10.2514/6.2018-3827>.
- [26] Althaus, D., “Niedriggeschwindigkeitsprofile: Profilentwicklungen und Polarenmessungen im Laminarwindkanal des Instituts für Aerodynamik und Gasdynamik der Universität Stuttgart,” Vieweg, 1996.